Regenerative Brake and Slip Angle Control of Electric Vehicle with In-wheel Motor and Active Front Steering

Hiroshi Fujimoto[1]

1) The University of Tokyo, Graduate School of Frontier Sciences

Transdisciplinary Sciences Bldg. 613, 5-1-5,

Kashiwanoha, Kashiwa, Chiba, 227-8561, Japan (E-mail: fujimoto@k.u-tokyo.ac.jp)

ABSTRACT: Electric vehicles (EVs) have attractive potential not only for energy and environmental performance but also for vehicle motion control because electric motors have quick and measurable torque response. Recently, the authors' laboratory has developed a completely original EV which has active front and rear steering systems and high-torque direct-drive in-wheel motors in the all wheels. In this paper, the main features of this vehicle are briefly introduced and our recent studies on pitching control, slip-ratio control, and yaw-rate and slip-angle control with lateral force sensors are explained with experimental results.

KEY WORDS: Electric vehicle, In-wheel motors, Pitching and Slip ratio Control, Active steering

1. Introduction

As a solution of energy and environmental problems, electric vehicles (EVs) is paid to attention. In addition, from the point of view of control engineering, EVs including battery, fuel-cell, and (plug-in) hybrid vehicles have very attractive potential. Since electric motors and inverters are utilized in drive system, they have great advantages over internal combustion engine vehicles (ICEVs). These advantages can be summarized as follows,

1) Quick torque response

The torque response of electric motors is 100-500 times as fast as that of ICEVs.

2) Measurable motor torque

In ICEVs, it is difficult to accurately measure their output torque. On the other hand, the output torque of electric motor can be measured easily from current. Therefore, the state of the road can be estimated precisely.

3) Individual wheels control

By using in-wheel motors, each wheel can be independently driven. Then, individual wheel control can enhance the vehicle stability.

These advantages of electric motor enhance vehicle motion control in EVs [1] [3]. Our research group focus the merits of motors and we are researching on the motion control for the electric vehicles to achieve safety and comfort driving [4]. In this paper, our recent researches on pitching control for comfort braking [5] and slip-ratio control for emergent braking [6] are briefly introduced by using the regenerative brake of in-wheel motors. Finally, the advanced vehicle stability control method by active front steering [7] is explained.

Fig. 1 Experimental vehicle

2. Experimental vehicle

To verify the proposed control algorithm, an original electric vehicle 'FPEV2-Kanon' developed in our laboratory is used for the test vehicle. Fig. 1 and Fig. 2 show the test vehicle and its configuration.

2.1. In-wheel motors

The outer rotor type in-wheel motors made by Toyo Denki Seizo K.K., Ltd. are installed in two rear wheels as driving power-train. Table 1 shows the specification of the in-wheel motors. Because this motor adopts the direct drive system, the reaction force from the road is directly transfered to the motor without gear reduction and backlash. Then it can be said that this vehicle is ideal to examine the proposed estimation and control methods. Fig. 3 shows in-wheel motor and Fig. 4 shows motor configuration.

Recently, we installed in-wheel motors with much higher torque into two front wheels to develop control methods for 4WD EVs. However in this paper, only the results with rear in-wheel motors will be introduced for 2 wheels individual drive EVs.

2.2. Energy Storage

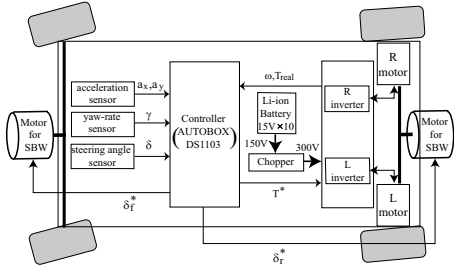The Li-ion battery is used for the energy storage. In this

Fig. 2 Configuration of FPEV2-Kanon
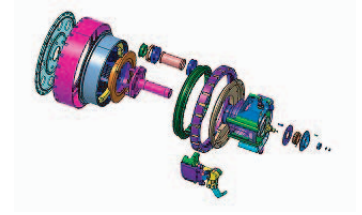

Fig. 3 In-wheel motor

Fig. 4 Motor configuration

Table 1 Specification of in-wheel motor

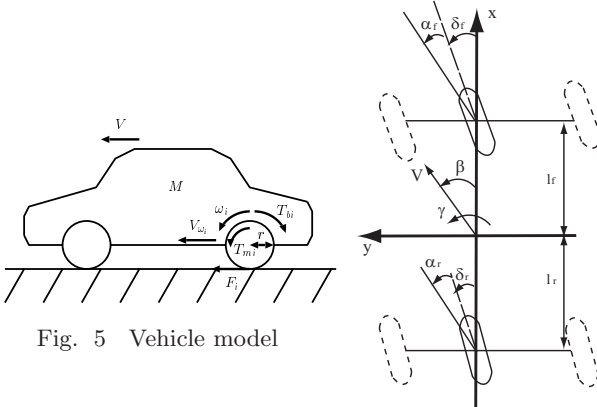| Manufacturer	TOYO DENKI
Type	Direct drive system
	Outer rotor type
Rated torque	137[Nm]
Maximum torque	340[Nm]
Rated power	4.3[kW]
Maximum power	10.7[kW]
Maximum speed	1500[rpm]
Weight	26[kg]
Cooling system	Air cooling

Fig. 5 Vehicle model

Fig. 6 Two wheel model

vehicle, ten batteries of 15V per module are installed and connected in series. In addition, the battery voltage 150V boosts to 300V by using chopper circuit, and it is fed to power to the inverter.

3. Vehicle modeling [(8)]

3.1. Longitudinal motion equation and slip ratio

By assuming that the driving resistance of the vehicle is negligible, the longitudinal motion equations both of wheel and vehicle shown in Fig. 5 can be described as

$$J_{\omega_i}\dot{\omega}_i = T_{mi} + T_{bi} - rF_i \tag{1}$$

$$m\dot{V} = 2F_f + 2F_r \tag{2}$$

$$V_{\omega i} = r\omega_i \tag{3}$$

where J_{ω_i} is the moment of inertia of wheel, ω_i is the motor angular velocity, T_{mi} is the motor torque, T_{bi} is the brake torque, r is the tire radius, F_i is the driving force generated by the contact between tire and road, m is the vehicle mass, V is the vehicle velocity, and $V_{\omega i}$ is the wheel velocity. The suffix $i = f, r$ represents the front wheel and rear wheel, respectively.

The slip ratio λ is defined as

$$\lambda = \frac{V_\omega - V}{\max(V_\omega, V, \epsilon)}, \tag{4}$$

where the denominator of (4) is changed by the values of V_ω and V. Because V_ω is faster than V when the vehicle is driving ($V_\omega > V$), the denominator becomes V_ω. On the other hand, because V_ω is slower than V on braking ($V_\omega < V$), it becomes V. Here, $\epsilon(\ll 1)$ is a small constant in order to avoid zero denominator.

3.2. Cornering force

The force in the orthogonal direction to the wheel side-slip angle is called the cornering force.

If the wheel side-slip angle is small, the cornering force increases in proportion to the wheel side-slip angle. If the wheel side-slip angle is big, the cornering force has nonlinear characteristic. Here, assuming that the wheel side-slip angle is small, the relationship between the cornering force and the wheel side-slip angle can be described as

$$F_{yf} \simeq Y_f = -C_f \alpha_f = -C_f\left(\beta + \frac{l_f}{V}\gamma - \delta_f\right) \tag{5}$$

$$F_{yr} \simeq Y_r = -C_r \alpha_r = -C_r\left(\beta - \frac{l_r}{V}\gamma - \delta_r\right), \tag{6}$$

where F_{yf} and F_{yr} are tire lateral forces, C_f and C_r are the cornering stiffness, α_f and α_r are tire side-slip angles, β is the vehicle side-slip angle, γ is the vehicle yaw-rate, l_f and l_r are the distance from body center of gravity to steering knuckle spindle and rear wheel axle. Y_f and Y_r are the cornering force of front and rear wheels which depend on the tire characteristics.

3.3. Two-wheel vehicle model

Fig. 6 shows the two-wheel vehicle model. This model is assumed that the roll of vehicle is negligible and the vehicle speed is constant. From the two-wheel vehicle model, the linearized dynamics of the lateral motion is derived as

$$mV\left(\frac{d\beta}{dt} + \gamma\right) = 2Y_f + 2Y_r$$
$$= -2C_f\left(\beta + \frac{l_f}{V}\gamma - \delta_f\right) - 2C_r\left(\beta - \frac{l_r}{V}\gamma\right), \tag{7}$$

$$I\frac{d\gamma}{dt} = 2l_fY_f - 2l_rY_r + N_z$$
$$= -2C_f\left(\beta + \frac{l_f}{V}\gamma - \delta_f\right)l_f + 2C_r\left(\beta - \frac{l_r}{V}\gamma\right)l_r + N_z, \tag{8}$$
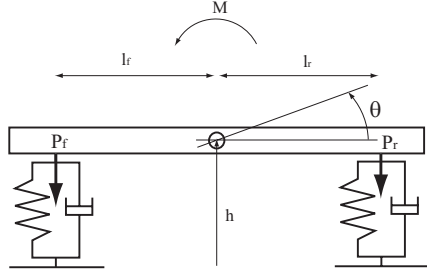
Fig. 7 Half car model

where I is the inertia around vehicle yawing axis, N_z is yaw-moment generated by the torque difference between left and right in-wheel motors.

4.   Pitching control [5]

This section focus on the pitching motion of the vehicle to enhance the driving comfort. The pitching motion occurs when the acceleration changes by the driving force and the braking force. We have studied on the control method of this pitching motion.

4.1. Modeling of the pitching motion

The pitching motion is body attitude change around the y axis of Fig. 6. Because the pitching motion is the motion around the y axis, it is possible to model it by the half car model, as shown in Fig. 7, which has only the front and rear wheels. The transfer function of the half car model can be described as

$$\frac{\theta}{M} = \frac{1}{I_p s^2 + C s + K}, \qquad (9)$$

where I_p is the pitching inertia, C is the damper coefficient, K is the spring constant, θ is the pitch angle, and M is the pitching moment around the center of gravity (COG). When the vehicle accelerates or decelerates, the pitching motion is caused. As the braking torque is transfered to the suspension through the brake unit, the anti-dive force is generated to front wheel and the anti-lift force is generated to rear wheel when the vehicle is braking. By considering them, (9) can be rewritten as

$$\theta = \frac{-2mh - m(\beta l_f \tan\phi_f + (1-\beta)l_r \tan\phi_r)}{I_p s^2 + C s + K} a_x, (10)$$

where the first term of right-hand side is generated by inertia force, the second term is caused by braking force which works at the contact point of tires, h is the height of COG, β is the front wheel distribution of braking force, and ϕ_f and ϕ_r are the angle from the contact point of tires to the instantaneous rotation centers of the suspension.

4.2. Control system design

(1)   Calculation of longitudinal acceleration

Because the obtained pitching model is acceleration input, the calculation method of acceleration from motor torque is considered. From (1) and (2), the acceleration is derived as follows.

$$a_{xn} = \frac{2T_{mi} - 2(J_{\omega_f}\dot{\omega}_f + J_{\omega_r}\dot{\omega}_r) - 4T_{bi}}{rm} \qquad (11)$$
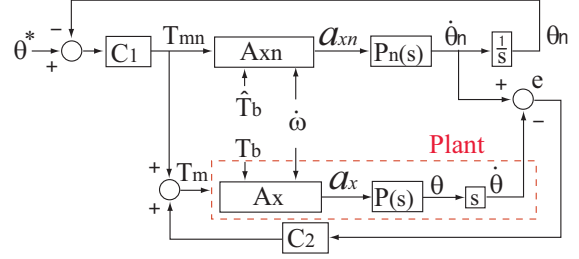

Fig. 8 Block diagram of pitching control

This equation can be calculated from motor torque, braking torque, and wheel acceleration. However, because it is generally difficult to measure the braking toque T_b directly, an estimation method of T_b is proposed.

(2)   Braking torque estimation

By eliminating F_i and V from (1) to (4), the equation of T_{bi} is derived as (12) when $V > V_{\omega_r}$. Here, the wheel acceleration $\dot{\omega}_r$ is obtained from the pseudo-derivative with high-pass filter. The braking torque estimation can be achieved precisely to consider the road condition because the slip ratio is included in (12).

$$\hat{T}_{bi} = \frac{1}{2}T_{mi} - \frac{1}{2}J_{\omega_r}\dot{\omega}_r - \frac{1}{2}J_{\omega_f}\dot{\omega}_f \\ - \frac{r^2 m \dot{\omega}_i}{4(1+\lambda_i)} + \frac{r^2 m \omega_i \dot{\lambda}_i}{4(1+\lambda_i)^2} \quad (12)$$

(3)   2DOF Pitching Controller

Based on the identified model of pitching motion and the estimation method of braking torque, pitching controller is proposed as shown in Fig. 8 which has two-degree-of-freedom (2DOF) control structure. The blocks A_x and A_{xn} represent (11). In this control system, the required sensors are the encoder of motors to detect ω_r (and $\dot{\omega}_r$) and gyroscope of pitch-rate $\dot{\theta}$. It is not appropriate to use the inverse plant model as the feedforward (FF) controller because the reference of pitch-angle is zero ($\theta^* = 0$) in this paper. Then, model following control structure is applied. In the FF control part of Fig. 8, the nominal plant $P_n(s)$ is controlled by the high-gain controller $C_1(s)$. This $C_1(s)$ generates the reference acceleration a_{xn} based on the braking torque estimation $\hat{T}_b$. The calculated reference of motor torque T_{mn} which can control pitch-angle of nominal plant ideally is applied to the real plant $P(s)$ as FF torque command. When the real plant coincides with the nominal model, the pitching motion can attenuate by this FF controller.

When the modeling error or disturbance exists, the pitch-rate error between nominal and real plants is appeared. This pitch-rate error is attenuated by the feedback controller $C_2(s)$ with moderate gain. Then, robust pitching control performance is achieved even when the modeling error exists.

Both $C_1(s)$ and $C_2(s)$ are designed by the pole placement method. Because the input of $C_1(s)$ is pitch-angle error, the

proportional-derivative (PD) controller is adopted as $C_1(s)$. On the other hand, the proportional-integral (PI) controller is applied as $C_2(s)$ since the input of $C_2(s)$ is pitch-rate error. The poles of closed-loop system with $C_1(s)$ can be set high enough to control pitch-angle of reference model ideally. However, those with $C_2(s)$ have limitation to keep the stability margin and noise attenuation of the actual closed-loop system with $P(s)$.

4.3. Experiments

The proposed control method is tested by experiments with 'FPEV2-Kanon'. The experiment is assumed that the vehicle is stopped by the mechanical brake while it is running about 9m/s on a flat dry road. When the vehicle speed becomes less than 1.5m/s, the pitching controller turns on. The parameters used in the experiment are the vehicle mass $m = 710$kg, the wheel radius $r = 0.302$m, the wheel inertia of the each front-rear wheel $J_{\omega r} = 1.26$Nms^2 and $J_{\omega f} = 1.0$Nms^2. As for the controllers C_1 and C_2, the poles of each closed-loop system are set to 14rad/s and 8rad/s, respectively.

Fig. 9 shows the experimental results. Fig. 9(a) and (b) show the pitch-rate and the pitch-angle which is obtained by the integral calculation of pitch-rate. Both the pitch-rate and the pitch-angle are suppressed compared with the case without control. From this results, it can be said that the comfortable braking is realized by the proposed control. Fig. 9(c) shows the estimated braking torque and the motor torque. The estimated braking torque is influenced by the sensor noise because the equations of braking torque estimation (12) include the wheel acceleration $\dot{\omega}$. The derivative calculation of the sensor signal amplifies the noise. Even though that, this noise does not damage the control performance of pitching motion severely as shown in Fig. 9(a) and (b).

Moreover, Fig. 9(d) shows the distance from beginning point of the breaking to the stop point with several experiments. This is obtained by the integral calculation of the vehicle speed. As the result, it can be said that the distance does not become longer by this control. This is very important for the application to the commercial products.

5. Slip ratio control on deceleration [6]

Authors' group proposed the slip ratio estimation method and the control method without the detection of the vehicle velocity at accelerating and decelerating in the references (4) and (9). In this paper, the slip ratio estimation and the control method without detection both of the vehicle velocity and the acceleration are extended to the two-dimensional motion when the vehicle is decelerating.

As for the friction coefficient between tire and road, the slip ratio becomes minimum value in near -0.2 as shown in

(a)Pitch-rate

(b)Pitch-angle (close-up)
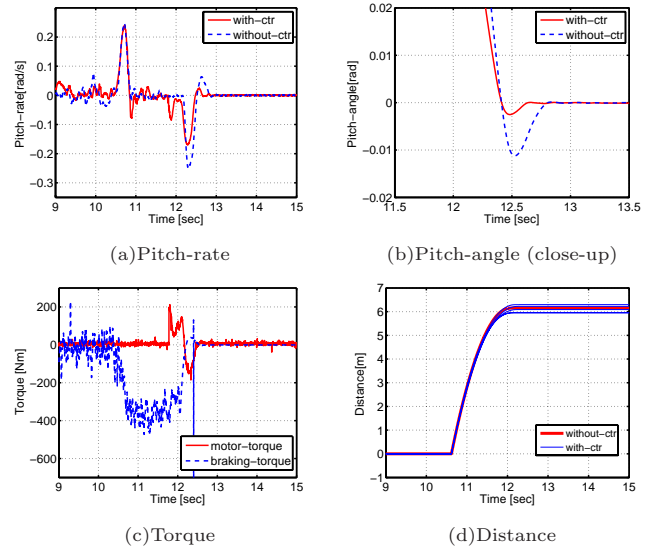
(c)Torque

(d)Distance

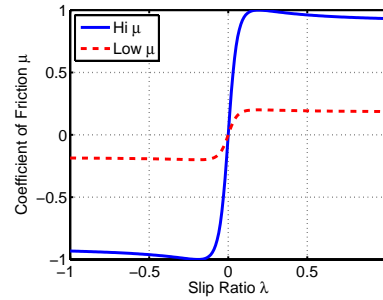Fig. 9 Experiment results of pitching control

Fig. 10 $\mu - \lambda$ curve

Fig. 10, and the maximum brake torque is obtained. Therefore, it can be said that the braking distance with control is shorter than the case without control if the wheel velocities are controlled to take the optimum slip ratio. However when the slip ratio approaches to -1, the vehicle motion becomes unstable and there are risks of side slip and spin.

First, estimation method of slip ratio without vehicle velocity is derived. Next, slip ratio control system is introduced.

5.1. Slip ratio estimation

By substituting from (1) to (3) into the time derivative of (4), the state equation on λ is obtained as

$$\dot{\lambda}_i = \frac{\dot{\omega}_i}{\omega_i}(1 + \lambda_i) - \left(\frac{T_m + T_b - J_\omega \dot{\omega}}{r^2 M \omega_i} \right)(1 + \lambda_i)^2 \quad (13)$$

where T_m, T_b and $J_\omega \dot{\omega}$ are as follows.

$$T_m = 2T_{mf} + 2T_{mr} \quad (14)$$
$$T_b = 2T_{bf} + 2T_{br} \quad (15)$$
$$J_\omega \dot{\omega} = 2J_{\omega_f} \dot{\omega}_f + 2J_{\omega_r} \dot{\omega}_r \quad (16)$$

Motor torque, brake torque and rotation speed of motor are obtained from motor current, pressure of brake line and resolver attached to motor, respectively. Moreover, the convergence of estimation error of the slip ratio is discussed in the reference (10).
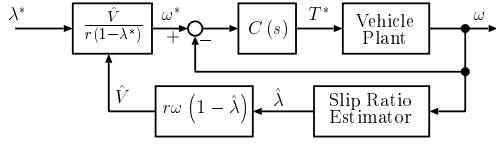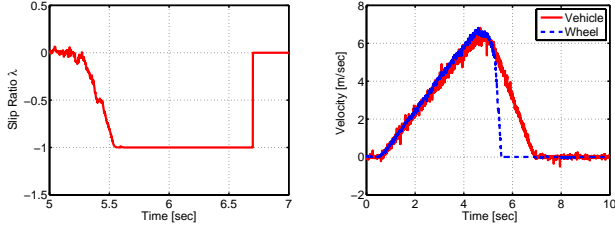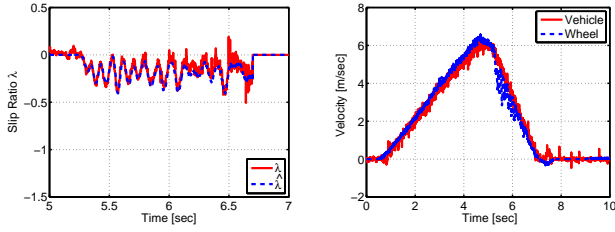
Fig. 11 Block diagram of slip ratio control

(a) Slip ratio   (b) Vehicle & wheel velocity

Fig. 12 Experiment results of slip-ratio control (without control)

(a) Slip ratio   (b) Vehicle & wheel velocity

Fig. 13 Experiment results of slip-ratio control (with control)

(a) Decoupling control

(b) LFO+YMO

Fig. 14 Block diagram of control system
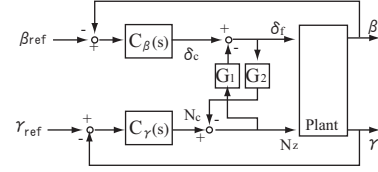
5.2. Slip ratio control

Next, the slip ratio control with the wheel speed control is designed. Because the wheel speeds can be detected with the resolver, the estimation of the slip ratio is equivalent to the estimation of the vehicle velocity. The estimated vehicle velocity can be calculated from (4) based on the estimated slip ratio. The reference value of wheel angular velocity at the optimum slip ratio is calculated from (17) and (18). Slip ratio is controlled by the wheel speed control, as shown in Fig. 11.

$$\hat{V} = \frac{r\omega}{1+\hat{\lambda}} \quad (17) \qquad \omega^* = \frac{1+\lambda^*}{r}\hat{V} \quad (18)$$
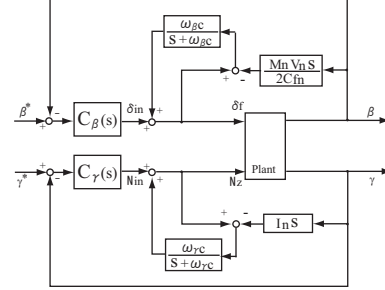
As the controller of the wheel velocity control, the simple PI-controller was used and the plant was assumed as

$$\omega = \frac{1}{J_\omega s}T, \qquad (19)$$

where the pole was located at -30rad/sec with the pole placement method and target slip ratio was -0.2. Experiments are carried out in playground of university. The vehicle decelerated only with the rear wheels both without control and with control because in-wheel motors were installed only rear wheel. Fig. 12 and Fig. 13 show experimental results. From Fig. 12, it can be confirmed that the wheels lock immediately with strong mechanical brakes and the slip ratio becomes -1 without control. From Fig. 13, wheels do not lock and the slip ratio converge to -0.2.

6. Yaw-rate and slip-slip angle control [7]

6.1. Decoupling control method

The vehicle side-slip angle and yaw-rate can be described as follows [8].

$$\begin{bmatrix} \beta \\ \gamma \end{bmatrix} = \begin{bmatrix} P_1(s) & P_2(s) \\ P_3(s) & P_4(s) \end{bmatrix} \begin{bmatrix} \delta_f \\ N_z \end{bmatrix} \qquad (20)$$

From this matrix, it is understood that two control inputs affect both the vehicle side-slip angle and yaw-rate. This interference influences the vehicle motion control. Then, the controller which takes into consideration this interference is designed. The control laws of the two control inputs are give as

$$\delta_f = \delta_c - G_1(s)N_z, \qquad (21)$$
$$N_z = N_c - G_2(s)\delta_f, \qquad (22)$$

where δ_c is the control steering angle, N_c is the control moment, $G_1(s)$ and $G_2(s)$ are the decoupling controllers. By substituting (21) and (22) for (20), we obtain

$$\beta = P_1(s)\delta_c + (P_2(s) - P_1(s)G_1(s))N_z,$$
$$\gamma = P_4(s)N_c + (P_3(s) - P_4(s)G_2(s))\delta_f.$$

Then the decoupling controller $G_1(s)$ and $G_2(s)$ can be designed as follows

$$G_1(s) = P_1^{-1}(s)P_2(s), \qquad (23)$$
$$G_2(s) = P_4^{-1}(s)P_3(s). \qquad (24)$$

The influence of the coupling terms are canceled. Fig. 14(a) is the block diagram of the decoupling control method.

6.2. Yaw-moment observer(YMO) [11]

By considering the disturbance moment N_d, (8) is rewritten as

$$I\frac{d\gamma}{dt} = 2l_f Y_f - 2l_r Y_r + N_d + N_z. \qquad (25)$$

Here N_d is the disturbance moment such as the road condition variation and the effect of crosswind. By defining the moment caused by lateral forces as $N_t := 2l_f Y_f - 2l_r Y_r$

and the lumped disturbance moment as $N_{td} := N_t + N_d$, (25) is simplified as

$$I\frac{d\gamma}{dt} = N_{dt} + N_z. \qquad (26)$$

By using the moment N_z as control input and yaw-rate γ as measured signal, the disturbance observer can be designed as Fig. 14(b). The authors named this specific disturbance observer as "yaw-moment observer (YMO)" in the reference (11). This YMO can compensate the lumped disturbance and nominalize the system as

$$\gamma = \frac{1}{I_n s} N_{in}. \qquad (27)$$

(27) is valid in the frequency band less than the cut-off frequency ω_c of YMO.

6.3. Lateral force observer (LFO)

By considering the disturbance lateral force, the lateral motion equation (7) is described as

$$mV\left(\frac{d\beta}{dt} + \gamma\right) = 2Y_f + 2Y_r + Y_d$$
$$= -2C_f\left(\beta + \frac{l_f}{V}\gamma - \delta_f\right) - 2C_r\left(\beta - \frac{l_r}{V}\gamma\right) + Y_d, (28)$$

where Y_d is the disturbance lateral force caused by road condition variation and crosswind. Here, Y_{td} is defined as

$$Y_{td} = -2C_f\left(\beta + \frac{l_f}{V}\gamma\right) - 2C_r\left(\beta - \frac{l_r}{V}\gamma\right) - mV\gamma + Y_d.$$

Then, (28) is rewritten as

$$mV\dot{\beta} = 2C_f\delta_f + Y_{td}. \qquad (29)$$

By using the front steering δ_f as control input and β as measured signal, the disturbance observer can be designed as Fig. 14(b). The authors named this specific disturbance observer as "lateral force observer (LFO)". This LFO can nominalize the dynamics as

$$\beta = \frac{2C_{fn}}{m_n V_n s}\delta_{in}. \qquad (30)$$

6.4. Experimental verification

The decoupling control method shown in Fig. 14(a) and the proposed control method combined YMO and LFO shown in Fig. 14(b) are compared by experiments.

In the proposed method, the controller $C_\beta(s)$ is simply designed by proportional control in which the pole of the closed loop is placed to -2.0rad/s for nominal plant (30). The controller $C_\gamma(s)$ is also designed by proportional controller in which the pole of the closed loop is placed to -1.0rad/s for nominal plant (27). The cut off frequency of LFO and YMO is set to 10rad/s.

In the decoupling control, $C_\beta(s)$ is designed by PID controller in which the poles of the closed loop are placed to -6.5rad/s for transfer function $P_1(s)$. $C_\gamma(s)$ is also designed by PID controller with -5.5rad/s closed-loop pole for transfer function $P_4(s)$. The parameters are set to vehicle speed is 12km/h, reference of vehicle side-slip angle is 0.035rad, and reference of yaw-rate is 0.15rad/s in experiments. In this paper, experiment vehicle runs on non-pavement road where the grip is lower than the asphalt road at $V=12$ km/h. The vehicle side-slip angle is measured with optical sensor CORREVIT S-400 of the DATRON Co., Ltd.

Fig. 15 shows the experimental results without parameter error in cornering stiffness (CS). Fig. 16 is the case with the 70 % parameter error. As shown in Fig. 15, both the conventional method (decoupling control) and the proposed method (LFO+YMO) track the references of yaw-rate and side-slip angle in the case without parameter variation. On the other hand, in the case with parameter error the conventional method becomes highly oscillatory because the decoupling controllers (23) and (24) highly depend on the values of CS. On the other hand, the proposed controllers do not depend on these values except for C_{fn} in (30), almost same response with Fig. 15 is obtained even with the parameter variation, as shown in Fig. 16. The small vibration is caused by the roughness of the non-pavement road.

Therefore, it can be said that the proposed method achieves higher robustness to the CS variation than the conventional method.

7. Conclusion

In this paper, our original EV is explained, which has direct drive in-wheel motors and active steering systems. Moreover, our recent studies on pitching, braking, yawing, and side-slip are introduced with experimental results.

Acknowledgment

References

(1) Y.Hori: "Future Vehicle Driven by Electricity and Control-Research on Four-Wheel-Motored: UOT Electric March II", IEEE Trans. IE, Vol.51, No. 5, 2004

(2) M.Kamachi, K.Walters: "A Research of Direct Yaw-Moment Control on Skippery Road for In-Wheel Motor Vehicle", EVS-22 Yokohama, JAPAN, Oct.23-28, pp.2122-2133, 2006

(3) H.Sugai, S.Murata: "Influence of In-wheel-motor to vehicle structure and suspension", JSAE Annual Congress, No. 0105173, 2010

(4) H.Fujimoto, K.Fujii, N.Takahashi: "Road Condition Estimation and Motion Control of Electric Vehicle with In-wheel Motors", JSAE Annual Congress, pp. 25-28, 2006

(5) H.Fujimoto, S.Sato: "Pitching Control Method Based on Quick Torque Response for Electric Vehicle", in Proc. International Power Electronics Conference -ECCE ASIA-, pp. 801–806, 2010

(6) T.Suzuki, H.Fujimoto: "Slip Ratio Estimation and Regenerative Brake Control without Detection of Vehicle Velocity and Acceleration for Electric Vehicle at Urgent Brake-turning", in Proc. The 11th IEEE International Workshop on Advanced Motion Control Proceedings, Niigata, pp.273-278, 2010

(7) H.Fujimoto, Y.Yamauchi: "Advanced Motion Control of Electric Vehicle Based on Lateral Force Observer with Active Steering", in Proc. IEEE International Symposium
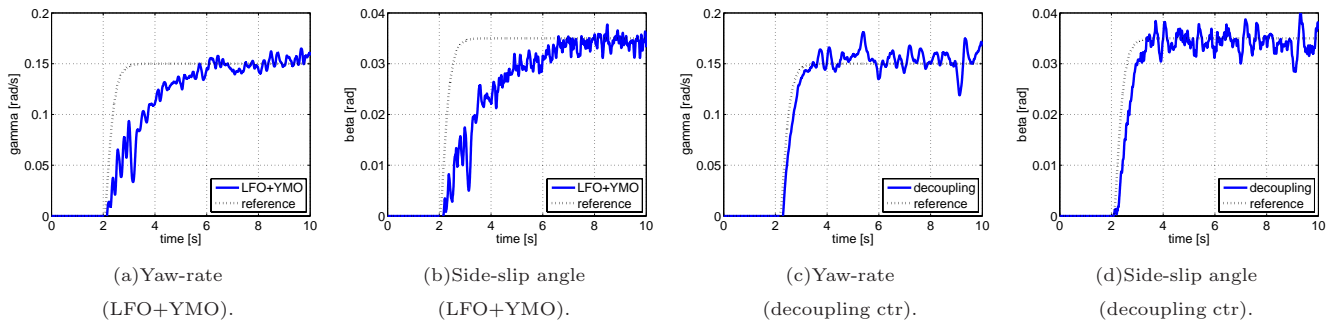
(a)Yaw-rate
(LFO+YMO).

(b)Side-slip angle
(LFO+YMO).

(c)Yaw-rate
(decoupling ctr).

(d)Side-slip angle
(decoupling ctr).

Fig. 15 Experiment results (CS with true value).

(a)Yaw-rate
(LFO+YMO).

(b)Side-slip angle
(LFO+YMO).

(c)Yaw-rate
(decoupling ctr).
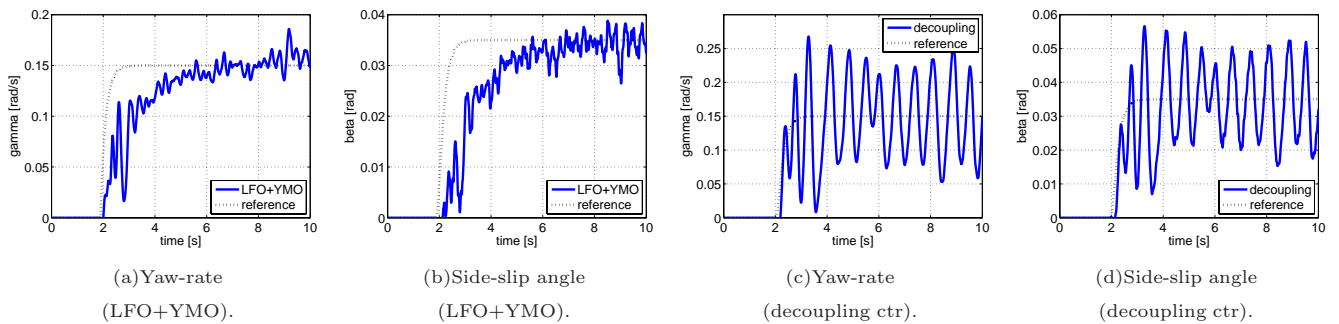
(d)Side-slip angle
(decoupling ctr).

Fig. 16 Experiment results (CS with parameter error).

on Industrial Electronics 2010 Proceedings, Bari, Italy, pp.3627-3632, 2010.

(8) R. Rajamani: "Vehicle Dynamics and Control", Springer Science & Business Media, Inc., 2006

(9) K.Fujii, H.Fujimoto: "Traction Control based on slip ratio estimation for Electric Vehicle", in Proc. The Fourth Power Conversion Conference, Nagoya, pp.688-693, 2007

(10) T.Suzuki, H.Fujimoto: "Proposal of Slip Ratio Estimation Method without Detection of Vehicle Speed for Electric Vehicle on Deceleration", IEE of Japan Technical Meeting Record, VT-07-24, pp. 77-82, 2007 (in Japanese)

(11) H.Fujimoto, T.Saito, T.Noguchi: "Motion Stabilization Control of Electric Vehicle under Snowy Conditions Based on Yaw-Moment Observer", in Proc. 8th IEEE International Workshop on Advanced Motion Control (AMC'04), Kawasaki, pp.35-40, 2004